

Colloidal domain lithography for regularly arranged artificial magnetic out-of-plane monodomains in Au/Co/Au layers

This article has been downloaded from IOPscience. Please scroll down to see the full text article.

2011 Nanotechnology 22 095302

(<http://iopscience.iop.org/0957-4484/22/9/095302>)

View [the table of contents for this issue](#), or go to the [journal homepage](#) for more

Download details:

IP Address: 130.209.6.41

The article was downloaded on 05/04/2012 at 17:59

Please note that [terms and conditions apply](#).

# Colloidal domain lithography for regularly arranged artificial magnetic out-of-plane monodomains in Au/Co/Au layers

Piotr Kuświk<sup>1</sup>, Arno Ehresmann<sup>2</sup>, Maria Tekielak<sup>3</sup>,  
Bogdan Szymański<sup>1</sup>, Iosif Sveklo<sup>3</sup>, Piotr Mazalski<sup>3</sup>,  
Dieter Engel<sup>2</sup>, Jan Kisielewski<sup>3</sup>, Daniel Lengemann<sup>2</sup>,  
Maciej Urbaniak<sup>1</sup>, Christoph Schmidt<sup>2</sup>, Andrzej Maziewski<sup>3</sup> and  
Feliks Stobiecki<sup>1</sup>

<sup>1</sup> Institute of Molecular Physics, Polish Academy of Sciences, M. Smoluchowskiego 17, 60-179 Poznań, Poland

<sup>2</sup> Institute of Physics and Centre for Interdisciplinary Nanostructure Science and Technology, University of Kassel, Heinrich-Plett-Strasse 40, D-34132 Kassel, Germany

<sup>3</sup> Laboratory of Magnetism, Faculty of Physics, University of Białystok, Lipowa 41, 15-424 Białystok, Poland

E-mail: [kuswik@ifmpan.poznan.pl](mailto:kuswik@ifmpan.poznan.pl)

Received 26 July 2010, in final form 22 December 2010

Published 24 January 2011

Online at [stacks.iop.org/Nano/22/095302](http://stacks.iop.org/Nano/22/095302)

## Abstract

Regularly arranged magnetic out-of-plane patterns in continuous and flat films are promising for applications in data storage technology (bit patterned media) or transport of individual magnetic particles. Whereas topographic magnetic structures are fabricated by standard lithographical techniques, the fabrication of regularly arranged artificial domains in topographically flat films is difficult, since the free energy minimization determines the existence, shape, and regularity of domains. Here we show that keV He<sup>+</sup> ion bombardment of Au/Co/Au layer systems through a colloidal mask of hexagonally arranged spherical polystyrene beads enables magnetic patterning of regularly arranged cylindrical magnetic monodomains with out-of-plane magnetization embedded in a ferromagnetic matrix with easy-plane anisotropy. This colloidal domain lithography creates artificial domains via periodic lateral anisotropy variations induced by periodic defect density modulations. Magnetization reversal of the layer system observed by magnetic force microscopy shows individual disc switching indicating monodomain states.

(Some figures in this article are in colour only in the electronic version)

## 1. Introduction

Bit patterned media, displaying regular arrangements of magnetic monodomains with out-of-plane anisotropy, of defined shape, size, and at defined positions are holding promise to be applied in a new generation of magnetic storage media [1–3]. Moreover, regularly arranged magnetic domains with varying widths in an external magnetic field have been used for the transport of individual magnetic particles, enabling completely new possibilities in biotechnology or particle sorting by magnetophoresis [4]. For both fields the final goal is to fabricate patterns of individually switchable monodomain areas with negligible effect of mutual interactions

on the magnetic reversal. Topographically separated magnetic patterns have been fabricated by ‘top down’ approaches applying lithographical techniques [5–8] or by ‘bottom up’ approaches using self-assembly [9–11] (block-copolymer lithography [12]) or colloidal lithography [13, 14], mostly combined with an etching step. However, regularly spaced artificial magnetic out-of-plane domains in a continuous and flat layer system are difficult to fabricate, since the existence of domains, their shape, and regularity is usually determined by free energy minimization and is, therefore, characteristic for a certain material or layer system. Moreover these naturally occurring domains are usually not arranged in regular dot patterns at defined places, except for some well known

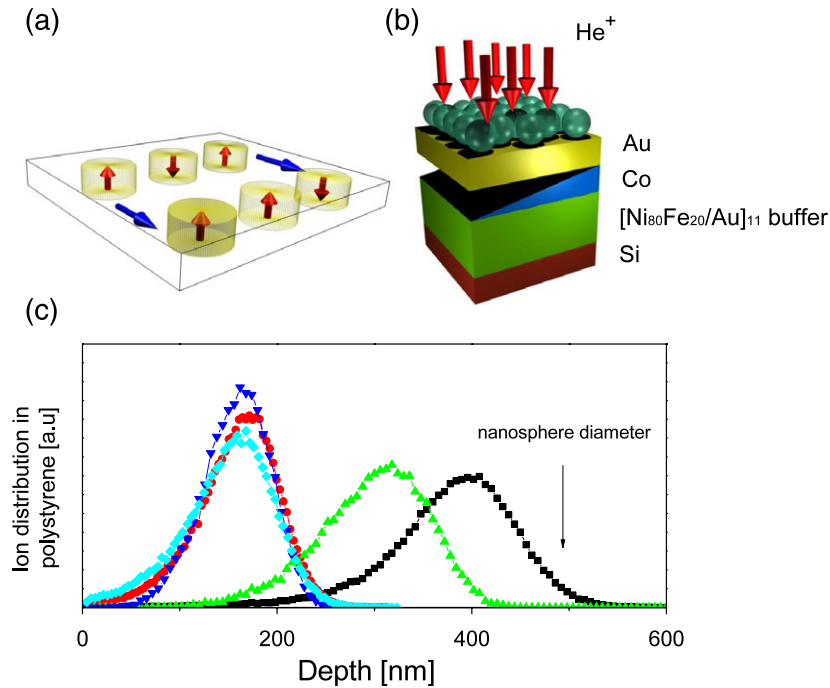


**Figure 1.** (a) Sketch of the envisaged cylindrical out-of-plane domains of defined diameter at regularly arranged positions embedded in an easy-plane ferromagnetic matrix. (b) Layer system and sketch of the colloidal domain lithography used in the experiments. (c) SRIM simulation of the implanted ion depth distribution in polystyrene when bombarded by 10 keV He<sup>+</sup> (red circles), 30 keV He<sup>+</sup> (black squares), 100 keV Ar<sup>+</sup> (blue down triangles), and 200 keV Ar<sup>+</sup> (green up triangles) ions and polystyrene covered by 3 nm Au bombarded by 10 keV He<sup>+</sup> ions (cyan diamonds).

bubble domain patterns in garnet films [4] and usually do possess small correlation lengths. In a pioneering work Chappert [15] showed that light ion bombardment of Co/Pt thin film systems through masks results in artificial out-of-plane domains by local anisotropy modifications such that for large ion fluence the perpendicular magnetic anisotropy (PMA) transforms into easy-plane [15–17]. Recently also the reverse effect, i.e. the increase of PMA by ion bombardment has been observed [18]. For data storage applications, particularly interesting are planar magnetic heterostructures (e.g. Co/Pt, Co/Au) [16, 19] with a regular arrangement of artificial monodomains with PMA embedded in a non-ferromagnetic matrix or in a matrix with, for example, easy-plane anisotropy. Since usually ion bombardment causes a degradation of PMA in Co/Pt and Co/Au films, bombardment through stencil masks results in regularly arranged, separate areas with easy-plane anisotropy embedded in a matrix with PMA. When defects are neglected, positions and shapes of the naturally occurring domains are determined by the free magnetic energy minimization of the layer system and are thus depending on layer thickness, anisotropy constants, exchange and magnetostatic coupling [20], and, in the case of multilayers, on the repetition numbers [21]. Here we show that the characteristics of an Au/Co/Au thin film system on a NiFe/Au buffer enables patterning of regularly ordered cylindrical magnetic monodomains with strong PMA, in a continuous easy-plane anisotropy ferromagnetic matrix (figure 1(a)) when magnetic patterning by light ion bombardment is combined with colloidal lithography (figure 1(b)), establishing colloidal domain lithography. The regular anisotropy modulations

induced in this continuous layer system are caused by regular defect density modulations and result in regular patterns of cylindrical domains with defined diameters and with large correlation lengths.

## 2. Experimental details

For the experiments, two (nominally identical) [Ni<sub>80</sub>Fe<sub>20</sub> (2 nm)/Au(3 nm)]<sub>11</sub>/Co(wedge)/Au(3 nm) layer systems (A and B) have been deposited, onto naturally oxidized Si(100) substrates, by UHV magnetron sputtering (base pressure: 10<sup>-9</sup> mbar) using Ar as the process gas with a deposition pressure of 10<sup>-4</sup> mbar. The thickness of the Co layer was linearly varied between 0 and 2 nm along the sample with a gradient of 0.2 nm mm<sup>-1</sup>, which was realized by a movable shutter in the deposition chamber in the vicinity of the substrate, moving with constant velocity during deposition. The [Ni<sub>80</sub>Fe<sub>20</sub>(2 nm)/Au(3 nm)]<sub>11</sub> buffers cause well textured Au(111) layers and in consequence PMA of the Co layer is observed in a relatively large range of Co thicknesses (up to 1.7 nm [17]). Additionally, the soft magnetic layer (Ni<sub>80</sub>Fe<sub>20</sub>) closes the magnetic flux and generates stronger stray fields over the Co layer, important for magnetic force microscopy (MFM) measurements as well as in perpendicular recording systems [3]. The thicknesses of the Au layers (3 nm) have been chosen to avoid interlayer exchange coupling between adjacent magnetic layers [22]. Ion bombardment has been performed by 10 keV He<sup>+</sup> ions from a home built plasma source with fluences specified in the text. All magnetic characterizations have been performed *ex situ* at room temperature. The Kerr

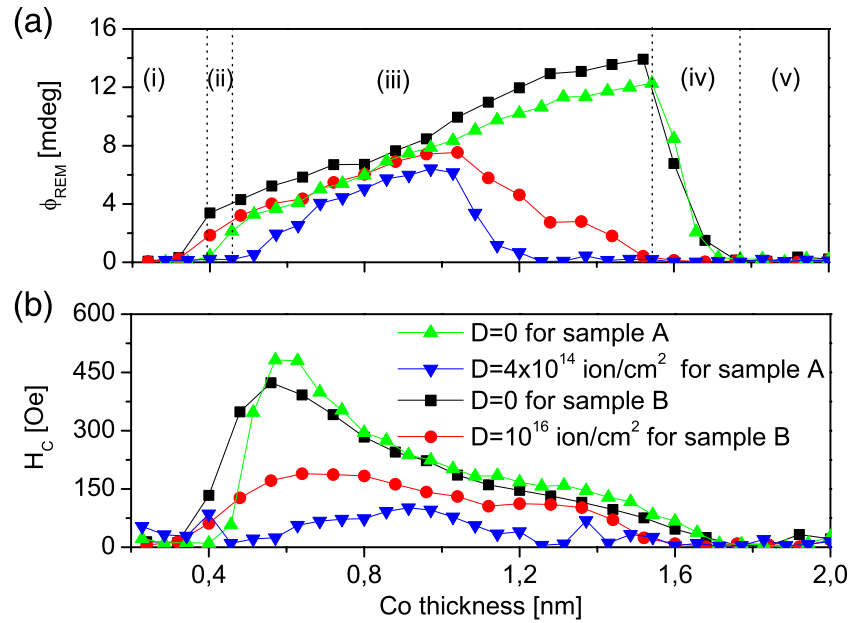


**Figure 2.** Remnant Kerr rotation  $\phi_{\text{REM}}$  (a) and coercive field  $H_C$  (b) for a magnetic field  $H_{\text{ext}}$  applied perpendicular-to-plane for sample A (without mask) and sample B (covered by the colloidal mask) in the as-deposited states and after ion bombardment with different  $\text{He}^+$  ion fluences, as functions of the Co layer thickness.

rotation  $\phi$  as a measure of the polar magnetization component as a function of a magnetic field  $H_{\text{ext}}$  applied perpendicularly to the sample plane has been measured by a polar magneto-optic Kerr-effect (P-MOKE) magnetometer at a laser wavelength of 640 nm and with a spot diameter of 0.5 mm. MFM images have been taken by an NT-MDT NTEGRA system, equipped with low magnetic moment MFM tips (MESP-LM, Veeco). Images have been taken in tapping/lift mode, enabling the recording of both topography and a map of magnetic interactions between sample and tip. Demagnetization of the samples has been carried out in an alternating field with decreasing amplitude.

Sample A has been used for basic investigations of the 10 keV  $\text{He}^+$  ion bombardment influence on the magnetic properties of the Co layers with different thicknesses. No colloidal mask has been deposited on sample A.

Sample B has been used to prove the feasibility of colloidal domain lithography by depositing a colloidal mask of 470 nm diameter polystyrene beads on the sample surface in a closely packed hexagonal lattice (figure 1(b)) and bombarding it by 10 keV  $\text{He}^+$  ions with a fluence of  $10^{16}$  ions  $\text{cm}^{-2}$ . Charging of the polystyrene beads has been prevented by capping the beads by a 3 nm thick Au layer. The colloidal mask has been prepared by deposition of polystyrene beads (Invitrogen) of 470 nm diameter by self-assembly through dip coating [23, 24] (figure 1(b)). After ion bombardment and prior to magnetic characterization, the nanospheres were washed out in an ultrasonic cleaner using tetrahydrofuran (THF). The optimum Co layer thickness for this technique has been determined after removal of the bead mask by analysis of MFM images and P-MOKE measurements as functions of the Co layer thickness. SRIM [25] simulations (figure 1(c)) show that the full diameter of the beads protects the layers beneath from 10 keV  $\text{He}^+$  ion penetration, however, the spherical bead shapes ensure gradual transitions between areas subjected

to full dose ion penetration and protected areas. It is also evident from figure 1(c) that 10 keV  $\text{He}^+$  ion bombardment may be replaced by 100 keV  $\text{Ar}^+$  ion bombardment in terms of implanted ion depth distribution and that covering beads by the 3 nm Au layer does not significantly change the implanted ion depth distribution.

### 3. Results and discussions

#### 3.1. Magnetic properties' dependence of the Au/Co(wedge)/Au layer system on the Co layer thickness prior to bombardment

The remnant Kerr rotation angle  $\phi_{\text{REM}}$  and the coercive field  $H_C$  as a function of  $t_{\text{Co}}$  prior to bombardment determined by P-MOKE for sample A are displayed in figures 2(a) and (b), respectively (green up triangles). The layer system without colloidal mask displays five distinct ranges of  $t_{\text{Co}}$  with different magnetic properties of the Co layer.

- (i)  $t_{\text{Co}} \lesssim 0.4$  nm,  $\phi_{\text{REM}} = 0$ : the Co layer is paramagnetic or superparamagnetic or both phases coexist.
- (ii)  $0.4$  nm  $\lesssim t_{\text{Co}} \lesssim 0.5$  nm,  $\phi_{\text{REM}} > 0$ : in this  $t_{\text{Co}}$  range  $\phi_{\text{REM}}$  increases faster with  $t_{\text{Co}}$  as compared to the linear dependence of  $\phi_{\text{REM}}(t_{\text{Co}})$  for higher Co thicknesses (range iii). The Co layer most probably consists of superparamagnetic and ferromagnetic clusters with PMA.
- (iii)  $0.5$  nm  $\lesssim t_{\text{Co}} \lesssim 1.5$  nm,  $\phi_{\text{REM}}$  increases linearly with  $t_{\text{Co}}$ : the Co layer is magnetically continuous and ferromagnetic, characterized by strong PMA with a maximum of  $H_C$  for  $t_{\text{Co}} \approx 0.6$  nm ( $H_C \geq 400$  Oe).
- (iv)  $1.5$  nm  $\lesssim t_{\text{Co}} \lesssim 1.7$  nm,  $\phi_{\text{REM}}(t_{\text{Co}})$  abruptly decreases to zero: the Co layer undergoes a spin reorientation transition (SRT) from perpendicular to easy-plane anisotropy via an 'easy cone' configuration [26].

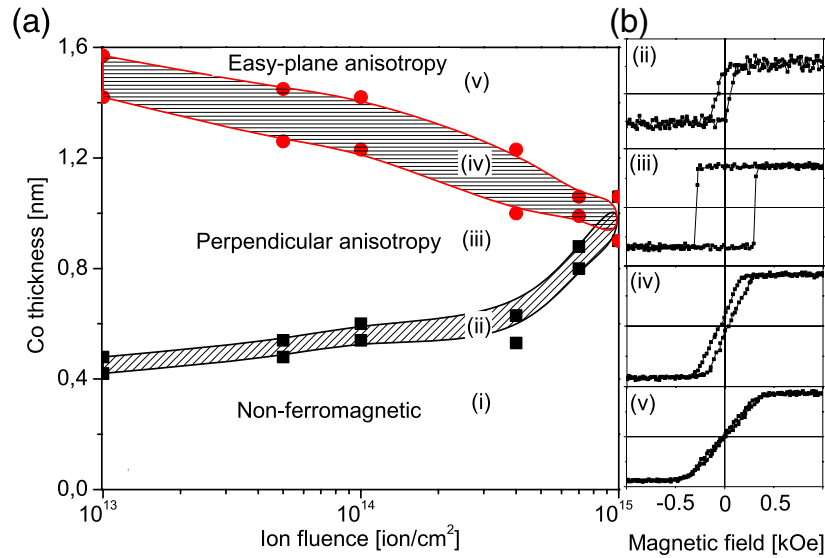


**Figure 3.** Magnetic phase changes of the Co layer as a function of Co layer thickness caused by bombardment with 10 keV  $\text{He}^+$  ions. (a) Variation of the Co thickness intervals (i)–(v) as a function of  $\text{He}^+$  ion fluence. (b) Hysteresis loops corresponding to thickness intervals (ii)–(v). Dashed areas (ii) and (iv) are guides to the eye for the transition regimes.

(v)  $t_{\text{Co}} \gtrsim 1.7$  nm: the effective anisotropy of Co is easy-plane.

Characteristic P-MOKE hysteresis loops for ranges (ii)–(v) are displayed in figure 3(b).

### 3.2. Magnetic property changes of the Au/Co(wedge)/Au layers by ion bombardment

For sample A, range (iii) of  $t_{\text{Co}}$  decreases after bombardment with increasing ion fluence  $D$  (see figures 2 and 3(a)). This range disappears for  $D = 10^{15} \text{ He}^+ \text{ cm}^{-2}$ . Simultaneously the thickness ranges (i) related to non-ferromagnetic behavior and (v) related to easy-plane anisotropy increase with  $D$ . The  $t_{\text{Co}}$  range where the anisotropy changes from out-of-plane to easy-plane (iv) remains very narrow (less than 0.2 nm), i.e. the transition from range (iii) to (v) is almost independent of the ion fluence (figure 3(a)). These magnetic property changes of the Co layer are mainly related to short-range ion bombardment induced atomic displacements [27].

For  $t_{\text{Co}} \leq 0.9$  nm a fluence  $D = 10^{15} \text{ He}^+ \text{ cm}^{-2}$  is high enough to disrupt the continuity of the Co layer and paramagnetic or superparamagnetic clusters are formed embedded in the Au matrix. Figure 3(a) shows that the layer system undergoes a transition from range (iii) to range (i) of its magnetic characteristics. For  $t_{\text{Co}} > 0.9$  nm the effective PMA is reduced due to the decrease of surface anisotropy, possibly caused by increasing surface roughness and/or strain relaxation [28] (mixing between Au and Co is rather unlikely due to the immiscibility of both elements [19], however, according to the theoretical predictions [29], for thin film systems this process cannot be totally excluded). As a consequence the magnetization reorientation from perpendicular to easy-plane takes place for high  $t_{\text{Co}}$  at relatively low  $D$  (e.g. for  $t_{\text{Co}} = 1.4$  nm at  $D = 5 \times 10^{13} \text{ He}^+ \text{ cm}^{-2}$ ) and for low  $t_{\text{Co}}$  at higher  $D$  (e.g. for  $t_{\text{Co}} = 1.1$  nm at  $D = 10^{15} \text{ He}^+ \text{ cm}^{-2}$ ).

### 3.3. Ion bombardment through a colloidal mask

Periodic magnetic anisotropy modulations were induced in sample B by ion bombardment through a colloidal mask with  $D = 10^{16} \text{ He}^+ \text{ cm}^{-2}$ .  $D$  has been chosen to be high enough to destroy the PMA for all Co thicknesses. Regions of the sample surface beneath the centers of the nanospheres are completely protected from bombardment (figure 1(c)), areas in between the beads are subjected to full fluence with a gradual transition between full fluence and full protection. The fluence gradient is difficult to estimate, since lateral variations in ion fluence and average ion energy are strongly affected by ion scattering in the mask [30]. For the following discussion we focus first on the Co layer thickness range  $0.5 \text{ nm} \leq t_{\text{Co}} \leq 1.1$  nm. The laterally averaged magnetic properties of the Co layer after ion bombardment through the mask observed by P-MOKE are characterized by reduced  $\phi_{\text{REM}}$  and  $H_C$ , however, the rectangular shape of the hysteresis loop is preserved (compare figure 4(a) with figure 3(b) (iii)). This suggests that the mechanism for magnetization reversal of the sample after ion bombardment is the same as for the as-deposited layer system, i.e. reversal by nucleation of domains followed by rapid domain wall propagation in relatively large areas [21, 31] (see figure 5 for  $t_{\text{Co}} = 0.8$  nm). The reduced value of  $H_C$  indicates the creation of additional low field nucleation centers [31], which are probably located at the borders of the paramagnetic or superparamagnetic areas. These non-ferromagnetic areas, bombarded with full fluence ( $10^{16} \text{ He}^+ \text{ cm}^{-2}$ ), are located in between the spheres and are separated from each other. Their presence explains the reduced value of the average  $\phi_{\text{REM}}$  within the P-MOKE laser–sample interaction area (see section 2).

For the Co thickness range  $1.1 \text{ nm} < t_{\text{Co}} \leq 1.4$  nm high fluences induce anisotropy changes from perpendicular to easy-plane. Therefore, here the PMA is preserved in cylindrical areas beneath the centers of the mask spheres

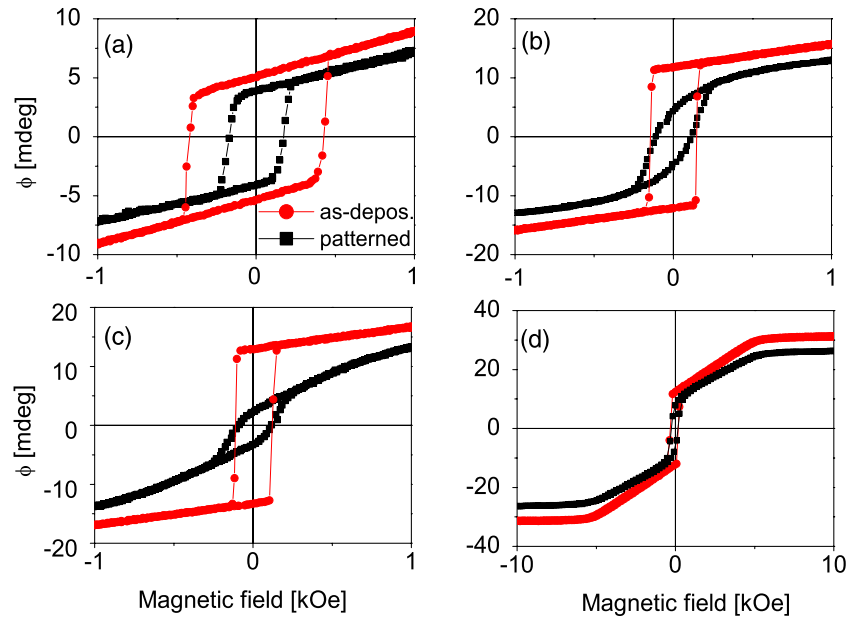


**Figure 4.** Exemplary P-MOKE hysteresis loops measured for different  $t_{\text{Co}}$  before and after  $\text{He}^+$  ion bombardment through the colloidal mask with  $D = 10^{16} \text{ He}^+ \text{ cm}^{-2}$ . (a)  $t_{\text{Co}} = 0.56 \text{ nm}$ ; (b)  $t_{\text{Co}} = 1.2 \text{ nm}$ ; (c)  $t_{\text{Co}} = 1.36 \text{ nm}$ ; (d)  $t_{\text{Co}} = 1.2 \text{ nm}$  in an extended magnetic field range. The linear part of (d) with saturation at 6 kOe corresponds to magnetization reversal of the buffer layer  $[\text{Ni}_{80}\text{Fe}_{20}(2 \text{ nm})/\text{Au}(3 \text{ nm})]_{11}$ , the central part to the one of the Co layer.

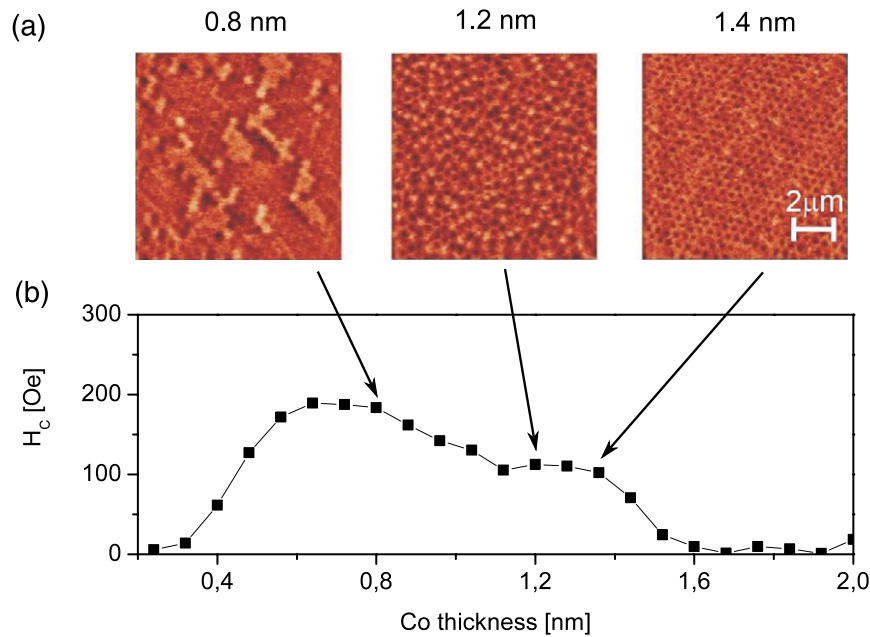


**Figure 5.** (a) MFM images in the demagnetized state of the  $\text{Au}(3 \text{ nm})/\text{Co-}t_{\text{Co}}/\text{Au}(3 \text{ nm})$  layer system (sample B) bombarded by  $10^{16} \text{ 10 keV He}^+ \text{ ions cm}^{-2}$  through a colloidal mask of 470 nm diameter polystyrene spheres for  $t_{\text{Co}} = 0.8, 1.2, 1.4 \text{ nm}$ . (b) Coercive field as a function of Co layer thickness for sample B after ion bombardment.

when bombardment by, for example, a fluence of  $D = 10^{16} \text{ He}^+ \text{ cm}^{-2}$  is performed. The rest of the cobalt layer forms a ferromagnetic matrix with easy-plane anisotropy, including areas with gradual anisotropy changes from out-of-plane to easy-plane. The diameters of the cylinders with PMA strongly decrease with increasing  $t_{\text{Co}}$  (figure 4) due to SRT at lower ion fluences, opening a way to tailor the diameters of the

artificial domains. This also explains the strong reduction of the average  $\phi_{\text{REM}}$  with  $t_{\text{Co}}$  (figures 2 and 4) for sample B because with increasing Co layer thickness the area with easy-plane anisotropy ( $\phi_{\text{REM}} = 0$ ) is increased at the expense of the area with PMA ( $\phi_{\text{REM}} = \phi_{\text{SAT}}$ ). The artificially introduced periodic domain patterns are stable in remanence, and their shape (cylindrical versus dendrite-like) and size

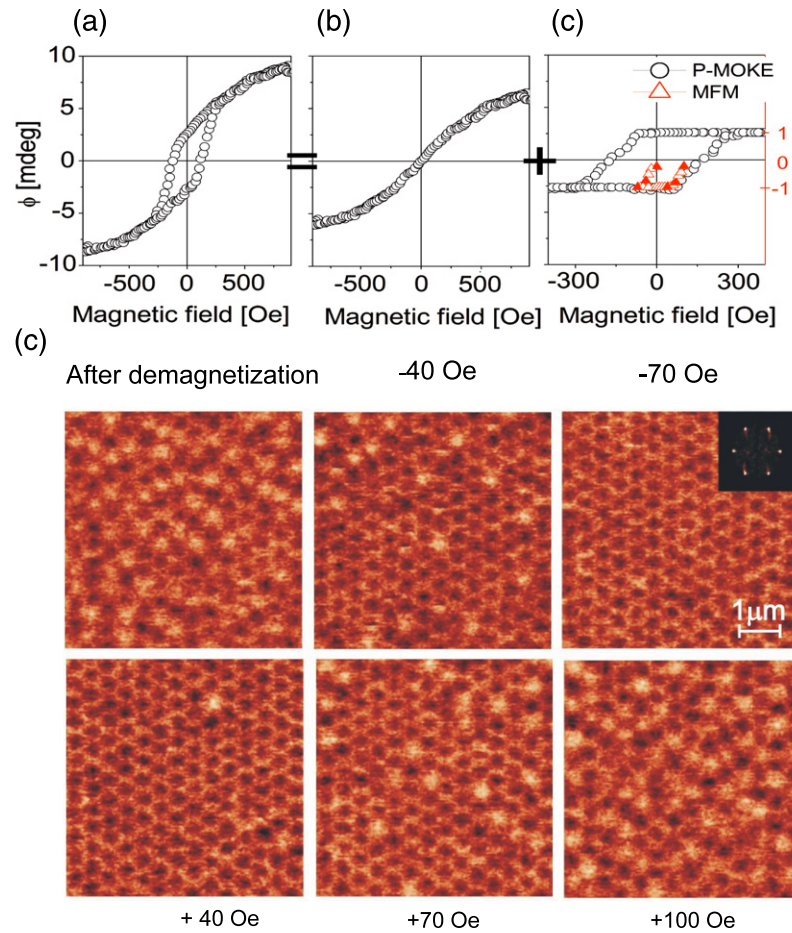


**Figure 6.** (a) P-MOKE hysteresis loop of sample B with  $t_{Co} \approx 1.25$  nm modified by ion bombardment through a colloidal mask corresponding to the Co layers magnetization only (see text). (b) Non-hysteretic part of the Co hysteresis loop in (a), corresponding to areas with easy-plane anisotropy (c), the difference between signals (a) and (b). Hysteresis loop corresponds to Co areas with PMA only. Full red triangles in (c) display the quantity  $1 - 2M_b/M$  calculated from the MFM images in (d) as described in the text (open triangles determined from images not shown). Note that the part of the hysteresis loop determined from MFM domain structure starts from the demagnetized state and is saturated first in the negative field. (d) Artificial magnetic domains for different external fields  $H_{ext}$  imaged by MFM. The inset shows the Fourier transform of the corresponding image.

(about 300 nm versus 5  $\mu$ m) are completely different to the naturally occurring domain structures [21, 31].

Areas with PMA of the demagnetized sample B imaged by MFM (figure 6) show two different contrasts, black and white, corresponding to the magnetization pointing parallel or antiparallel to the surface normal. The rest of the layer (with easy-plane anisotropy) is gray. In the demagnetized state the number of perpendicularly magnetized areas with magnetization up and down should be equal. This is almost true for films with  $1.1 \text{ nm} \leq t_{Co} \leq 1.3 \text{ nm}$  characterized by  $H_C > 100$  Oe (figures 5(a) and 6(d)). However, the summation of the respective areas in figure 6(d) indicates that there are some more black areas than white ones. This tendency is stronger for thicker Co layers, where  $H_C$  is lower. Indeed, for  $t_{Co} \geq 1.3$  nm MFM images recorded in remanence after demagnetization suggest that the magnetizations in almost all areas with PMA are oriented in the same direction (figure 5(a) for  $t_{Co} = 1.4$  nm). This domain orientation is caused by the stray field of the ferromagnetic probe tip during the MFM measurements.

The linear P-MOKE signal field dependence for high fields (in figure 4(d)  $1.5 \text{ kOe} \leq H_{ext} \leq 6 \text{ kOe}$  and  $-1.5 \text{ kOe} \geq H_{ext} \geq -6 \text{ kOe}$ ) corresponds to the magnetization reversal of the  $[\text{Ni}_{80}\text{Fe}_{20}(2 \text{ nm})/\text{Au}(3 \text{ nm})]_{11}$  buffer layer. Performing a linear fit in the above field range, interpolation for low field values, and subtracting this function from the measured P-MOKE signal  $\phi$  results in the loop of figure 6(a) characteristic for the magnetization reversal of the Co layer only. This loop has been disentangled in two contributions. The first unhysteretic one is related to Co areas with easy-plane anisotropy (figure 6(b)). This loop has then been subtracted from the one of figure 6(a) which results in the loop of figure 6(c). This loop shows reversal of Co areas with PMA, only. MFM images as a function of the magnetic field have been taken first from a demagnetized sample without magnetic field and then changing towards negative fields of up to  $-70$  Oe and finally towards positive fields of up to 100 Oe (figure 6(d)). The relative magnetization for each image has been determined from  $1 - 2M_b/M$ , where  $M_b$  is the number of black discs and  $M$  is the total number of discs within the field of view. These

values are displayed as red triangles in figure 6(c). The loop of figure 6(c) and the magnetic structure in figure 6(d) indicate that the switching of artificial domains occurs individually and is distributed within a relatively narrow field range (about 100 Oe).

#### 4. Summary

Light ion bombardment of a Au/Co/Au layer system with Co in a thickness range between  $1.1 \text{ nm} \leq t_{\text{Co}} \leq 1.3 \text{ nm}$  through a colloidal mask of polystyrene nanospheres enables magnetic patterning, resulting in a well ordered arrangement of cylindrical artificial domains with submicron diameters, PMA, and a coercive field  $H_C$  above 100 Oe. These artificial domains are separated from each other and embedded in a matrix with easy-plane anisotropy. They form an almost perfect two-dimensional hexagonal lattice in a continuous and flat layer system. The artificially introduced periodic domain patterns are stable in remanence, and the shape (cylindrical versus dendrite-like) and size (about 300 nm versus  $5 \mu\text{m}$ ) of the individual domains are completely different to the naturally occurring domain structures. The diameters and periodicity of these domains may be tailored by a variation of bead diameters, bead material, and ion fluence, demonstrating that colloidal domain lithography is a versatile tool for the fabrication of regularly arranged artificial domains with perpendicular anisotropies in continuous and flat layers for a multitude of applications.

#### Acknowledgments

Supported by the Polish State Committee for Scientific Research, grant no. N507287836 and N202235737. This work was partially financed by Polish–German joint project Technological-Cooperation. P K acknowledges a PhD grant from the Polish Academy of Sciences.

#### References

- [1] Prinz G A 1998 Magnetolectronics *Science* **282** 1660–3
- [2] Albrecht M, Hu G, Guhr I L, Ulbrich G C, Boneberg J, Leiderer P and Schatz G 2005 Magnetic multilayers on nanospheres *Nat. Mater.* **4** 203–6
- [3] Moser A, Takano K, Margulies D T, Albrecht M, Sonobe Y, Ikeda Y, Sun S and Fullerton E E 2002 Magnetic recording: advancing into the future *J. Phys. D: Appl. Phys.* **35** R157–67
- [4] Tierno P, Sagues F, Johansen T H and Fischer T M 2009 Colloidal transport on magnetic garnet films *Phys. Chem. Chem. Phys.* **11** 9615–25 and references therein.
- [5] Xiobin Z, Grütter P, Metlushko V and Ilic B 2002 Magnetization reversal and configurational anisotropy of dense permalloy dot arrays *Appl. Phys. Lett.* **80** 4789–91
- [6] Aign T, Meyer P, Lemerle S, Jamet J P, Ferré J, Mathet V, Chappert C and Bernas H 1998 Magnetization reversal in arrays of perpendicularly magnetized ultrathin dots coupled by dipolar interaction *Phys. Rev. Lett.* **81** 5656–9
- [7] Repain V, Jamet J P, Vernier N, Bauer M, Ferré J, Chappert C, Gierak J and Mailly D 2004 Magnetic interactions in dot arrays with perpendicular anisotropy *J. Appl. Phys.* **95** 2614–8
- [8] Todorovic M, Schultz S, Wong J and Scherer A 1999 Writing and reading of single magnetic domain per bit perpendicular patterned media *Appl. Phys. Lett.* **74** 2516–8
- [9] Burmeister F, Schäfle C, Keilhofer B, Bechinger C, Boneberg J and Leiderer P 1998 From mesoscopic to nanoscopic surface structures: lithography with colloid monolayers *Adv. Mater.* **10** 495–7
- [10] Ng V, Lee Y V, Chen B T and Adeyeye A O 2002 Nanostructure array fabrication with temperature-controlled self-assembly techniques *Nanotechnology* **13** 554–8
- [11] Langridge S et al 2006 Controlled magnetic roughness in a multilayer that has been patterned using a nanosphere array *Phys. Rev. B* **74** 014417
- [12] Choi D G, Jeong J R, Kwon K Y, Jung H T, Shin S C and Yang S M 2004 Magnetic nanodot arrays patterned by selective ion etching using block copolymer templates *Nanotechnology* **15** 970–4
- [13] Aizpurua J, Hanarp P, Sutherland D S, Käll M, Bryant G W and Garcia de Abajo F J 2003 Optical properties of gold nanorings *Phys. Rev. Lett.* **90** 057401
- [14] Yang S M, Jang S G, Choi D G, Kim S and Yu H K 2006 Nanomachining by colloidal lithography *Small* **2** 458–75
- [15] Chappert C et al 1998 Planar patterned magnetic media obtained by ion irradiation *Science* **280** 1919–22
- [16] Devolder T, Bernas H, Ravelosona D, Chappert C, Pizzini S, Vogel J, Ferré J, Jamet J P, Chen Y and Mathet V 2001 Beam-induced magnetic property modifications: basics, nanostructure fabrication and potential applications *Nucl. Instrum. Methods Phys. Res. B* **175–177** 375
- [17] Kuświk P, Kisielewski J, Weis T, Tekielak M, Szymański B, Urbaniak M, Dubowik J, Stobiecki F, Maziewski A and Ehresmann A 2008 He<sup>+</sup> ion bombardment induced effects on magnetic properties of Ni–Fe/Au/Co/Au films *Acta Phys. Pol. A* **113** 651–6
- [18] Jaworowicz J et al 2009 Spin reorientation transitions in Pt/Co/Pt films under low dose Ga<sup>+</sup> ion irradiation *Appl. Phys. Lett.* **95** 022502
- [19] Blon T, Ben Assayag G, Ousset J C, Pecassou B, Claverie A and Snoeck E 2007 Magnetic easy-axis switching in Co/Pt and Co/Au superlattices induced by nitrogen ion beam irradiation *Nucl. Instrum. Methods Phys. Res. B* **257** 374–8
- [20] Hellwig O, Berger J B, Kortright A and Fullerton E E 2007 Domain structure and magnetization reversal of antiferromagnetically coupled perpendicular anisotropy films *J. Magn. Magn. Mater.* **319** 13–55
- [21] Tekielak M, Mazalski P, Maziewski A, Schäfer R, McCord J, Szymański B, Urbaniak M and Stobiecki F 2009 Creation of out-of-plane magnetization ordering by increasing the repetitions number N in (Co/Au)<sub>N</sub> multilayers *IEEE Trans. Magn.* **44** 2850–3
- [22] Stobiecki F, Szymański B, Luciński T, Dubowik J, Urbaniak M and Röhl K 2004 Magnetoresistance of layered structures with alternating in-plane and perpendicular anisotropies *J. Magn. Magn. Mater.* **282** 32–8
- [23] Kosiorek A, Kandulski W, Chudziński P, Kempa K and Giersig M 2004 Shadow nanosphere lithography: simulation and experiment *Nano Lett.* **4** 1359–63
- [24] Kosiorek A, Kandulski W, Głaczyńska H and Giersig M 2005 Fabrication of nanoscale rings, dots, and rods by combining shadow nanosphere lithography and annealed polystyrene nanosphere masks *Small* **1** 439–44

- [25] Ziegler J F, Biersack J P and Littmark U 1985 *The Stopping and Range of Ions in Solids* (New York: Pergamon) [www.srim.org](http://www.srim.org)
- [26] Kisielewski M, Maziewski A, Tekielak M, Wawro A and Baczewski L T 2002 New possibilities for tuning ultrathin cobalt film magnetic properties by a noble metal overlayer *Phys. Rev. Lett.* **89** 087203
- [27] Fassbender J, Ravelosona D and Samson Y 2004 Tailoring magnetism by light-ion irradiation *J. Phys. D: Appl. Phys.* **37** R179–96
- [28] Aziz A, Bending S J, Roberts H, Crampin S, Heard P J and Marrows C H 2005 Artificial domain structures realized by local gallium focused ion-beam modification of Pt/Co/Pt trilayer transport structure *J. Appl. Phys.* **98** 124102
- [29] Guo H B, Li J H and Liu B X 2004 Atomistic modeling and thermodynamic interpretation of the bridging phenomenon observed in the Co–Au system *Phys. Rev. B* **70** 195434
- [30] Devolder T, Chappert C, Mathet V, Bernas H, Chen Y Y, Ravera H, Jamet J P and Ferré J 2000 Magnetization reversal in irradiation-fabricated nanostructures *J. Appl. Phys.* **87** 8671
- [31] Jamet J P *et al* 1998 Dynamics of the magnetization reversal in Au/Co/Au micrometer-size dot arrays *Phys. Rev. B* **57** 14320